Plasmonic based Electrochemiluminescence Biosensors

Subjects: Chemistry, Analytical

Contributor: Cheng Ma, Zhichen Zhang, Tingting Tan, Jun-Jie Zhu

Electrochemiluminescence (ECL) analysis has become a powerful tool in recent biomarker detection and clinic diagnosis due to high sensitivity and broad linear range. To improve the analytical performance of ECL biosensors, various advanced nanomaterials have been introduced to regulate ECL signal such as graphene, gold nanomaterials, quantum dots. Among these nanomaterials, some plasmonic nanostructures play important roles in the fabrication of ECL biosensors. The plasmon effect for ECL signal includes ECL quenching by resonant energy transfer, ECL enhancement by surface plasmon resonance enhancement, and change in the polarized angle of ECL emission. The influence can be regulated by the distance between ECL emitters and plasmonic materials, and the characteristic of polarization-angle-dependent surface plasmon coupling. This research outlines the recent advances of plasmonic based ECL biosensors involving various plasmonic materials include noble metals and semiconductor nanomaterials. The detection targets in these biosensors range from small molecules, proteins, nucleic acids, and cells thanks to the plasmonic effect. In addition to ECL biosensors, ECL microscopy analysis with plasmonic materials is also highlighted because of the enhanced ECL image quality by plasmonic effect. In the end, the future opportunities and challenges are discussed if more plasmonic effect will be introduced into ECL realm.

Keywords: plasmonic ; electrochemiluminescence ; biosensors

1. Introduction

As a member of the luminescence family, electrochemiluminescence (ECL) is a special form of chemiluminescence induced by redox reactions among electrogenerated high-energy radicals [1]. Because ECL does not depend on external light excitation, the adverse influence of autophotoluminescence and light scattering in analytical measurements can be avoided [2][3][4]. Compared with chemiluminescence techniques, ECL possess better spatial and temporal controllability for emission regions and time [5][6][7][8][9][10][11]. Therefore, more and more ECL biosensors have been developed due to its low light background, high sensitivity, and broad dynamic range [12][13][14][15]. The key point in the design of an ECL sensor is to optimize the performance of the luminophore or electrode substrate for the sake of enhanced ECL sensitivity [2][3][4][16][17][18][19][20]. Recently, various signal amplification methods have been proposed to improve the analytical properties of ECL sensors [4][12][13][16][21][22]. These approaches included using enzyme-mediated amplification, DNA-mediated amplification, new electrochemical catalytical substrate, and nanomaterial-assisted amplification [23][24]. Enzyme-mediated amplification used various enzymes to catalyze biochemical reactions and amplify the targets. Its merits include the flexible choice from abundant enzymes, high signal enhancement efficiency, and high selectivity. However, the vulnerable natural activity of enzymes can be more easily destroyed by harsh environments. DNA-mediated amplification is a kind of enzyme-free amplification technique by using DNA as the tool to improve the ECL signal. Thus, DNA-mediated amplification has better stability in a long term. However, most DNA amplification strategies rely on the hybridization of double stranded DNA, which is affected by the environment temperature. Electrochemical catalytical substrates can promote the electron transfer and surface area of the electrode, thereby enhancing ECL signals in some situations. Nanomaterial-assisted amplification can use nanomaterials as carriers of ECL emitters. Numerous ECL luminophores can be incorporated to carrier frameworks to provide much stronger ECL intensity for ultrasensitive biosensors. However, the uneven and heterogeneous nanocarriers may cause ECL signal deviation. In addition, luminophore leak and poor conductivity of the nanocarrier are problems to be solved. So far, many ECL-based biosensors with high sensitivity and selectivity have been fabricated to detect important analysts in the fields of environmental science, clinical diagnostics, food and water testing, and biowarfare agent detection [10]. In addition, ECL microscopy has become increasingly popular in analytical science due to its spatial and temporal resolution that has facilitated single-cell and single-particle analysis [25][26]. To briefly show the development history of ECL biosensors, researchers illustrated a roadmap for the progress of ECL biosensors and its future directions (**Figure 1**).

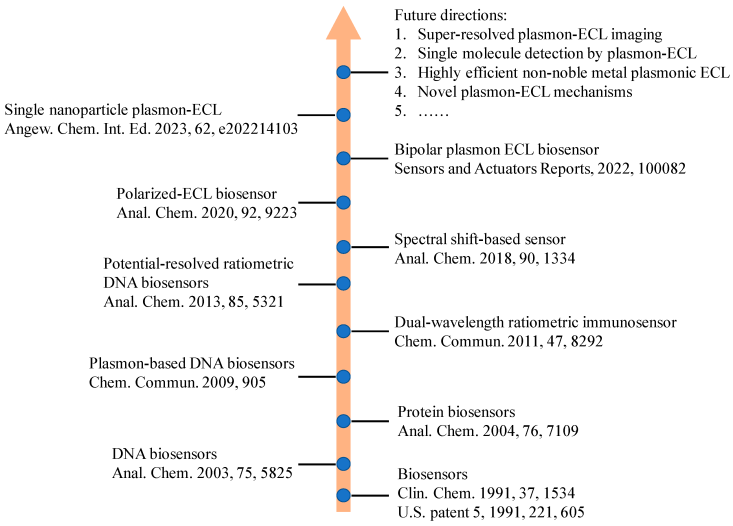

Figure 1. A roadmap for the progress of ECL biosensors and its future directions.

Surface plasmon resonance (SPR) occurs at the interface between a metal phase and a dielectric material [27][28]. After being excited by external optical radiation or in the presence of strong static electric and magnetic fields, a surface plasmon of the electrons at the surface of materials showed a collective oscillation wave, which propagated along the boundary between the dielectric and the metal. In addition, the SPR phenomenon was observed in not only noble metals but also in semiconductors such as MoS_2 [29][30]. The plasmonic effect has been widely used in many important fields such as photocatalysis, energy storage, and biosensors [31][32][33]. Localized surface plasmon resonance (LSPR) is a plasmon that oscillates locally around the nanoparticle. Therefore, LSPR is sensitive to changes in local dielectric environment. The effect of localized surface plasmon resonance (LSPR) has been well used in the detection of several biomolecules, including creatinine, cardiac troponin I, alanine aminotransferase, acetylcholine, cholesterol, uric acid, and p-cresol [34][35][36][37][38][39][40]. Optical emissions can be enhanced in the presence of the SPR effect, such as surface enhanced Raman scattering spectroscopy, total inner reflection, fluorescence, and chemiluminescence. Particularly, the molecular Raman scattering cross-section has an improved order-of-magnitude due to the excitation of collective electron oscillation of metal and semiconductor nanostructures [41][42][43][44]. Although surface enhanced Raman spectroscopy used noble metal nanostructures to enhance the Raman scattering signal from nearby molecules, an extrinsic probe is required for surface enhanced Raman spectroscopy. In fluorescent analytical methods, the distance between luminophores and metal nanostructures can cause the switch from fluorescence quenching to fluorescence enhancing [45][46]. The basic mechanism is the competition between the non-radiative transition in Forster resonance energy transfer and electromagnetic field enhancement. When a chromophore is in the evanescent field near metal surface, the large enhancement of fluorescence can occur where plasmon resonance reaches its maximum. However, photobleaching and photodamage are the roadblocks for plasmon-enhanced fluorescence methods. Recently, the plasmonic coupling and electromagnetic interaction exhibited tunable optical properties for ECL through regulating the distance between ECL emitters and plasmonic nanostructures. Due to the absence of an external light source, the ECL reactions at different plasmonic interfaces show different electrochemical rates and enhancement factors without the issue of photobleaching. Some studies involving ECL microscopy provided visualized evidence to characterize the plasmonic enhancement sites at the sub-particle level [47][48][49]. The surface plasmon also caused ECL polarization due to electron oscillation in the noble metals [50]. As a result, the ECL analytical performance can be improved if the polarized ECL signal can be used as the detection signal.

2. Fundamentals of Plasmon-Coupled ECL

Plasmon is the collective oscillation of conduction electrons in metals or semiconductors. Specifically, many noble metals and semiconductors have surface plasmon resonance properties. When ECL emission sites are very close to surface plasmons, the surface plasmons strongly interact with light. As a result, the ECL emission can be quenched or enhanced by the plasmonic effect, depending on the distance between the ECL emitter and plasmonic materials, as well as other factors. In addition, the polarization angle of ECL emission can be changed by the plasmonic effect. So far, the ECL emission can be regulated by two plasmon resonance effects including surface plasmon resonance (SPR) and localized surface plasmon resonance (LSPR). In terms of SPR, the most typical and widely used setup is the Kretschmann configuration, which uses thin gold film coated glass as the substrate. When the optimal beam is irradiated, metal substrates show strong surface plasmonic polarization (**Figure 2**). The resonance angle changed with the refractive index near gold film, which can be influenced by biomolecule recognition on gold film. Compared with SPR, LSPR is generated

on metal nanoparticles under light irradiation, which caused collective electron charge oscillations in metallic nanoparticles. In addition, the plasmonic effect is highly localized at the nanoparticles and decays quickly away from the nanoparticle. Therefore, many ECL biosensors used the distance-dependent LSPR effect to probe structure changes of DNA or a sandwiched immunoassay. For the plasmon coupled ECL system, SPR-based properties are highly dependent on the nanostructures of plasmonic materials. Metallic nanostructure arrays and porous metal membranes were wildly used as the source of plasmon because of their superior plasmonic properties and controllability via strategies of assembly and morphological regulation. The metallic nanostructures used in plasmon coupled ECL can improve ECL performance through the improvement of electrical conductivity, electro-catalytic activity, electromagnetic field enhancement, and so on. Xia et al. investigated the gold-coated polydimethylsiloxane chip by a stamping and spraying process [51]. The plasmonic gold microwells significantly enhanced ECL intensity for the analysis of intracellular glucose. Elena et al. has reported that ECL emission was related to the effective surface area of the nanoporous gold electrode [52]. Therefore, the nanoporous gold electrode possessed brighter ECL emission compared with the flat gold electrode. All in all, plasmonic materials with stable plasmonic performance, high specific surface area, multiple active sites, and good electrochemical properties played a key role in plasmon coupled ECL.

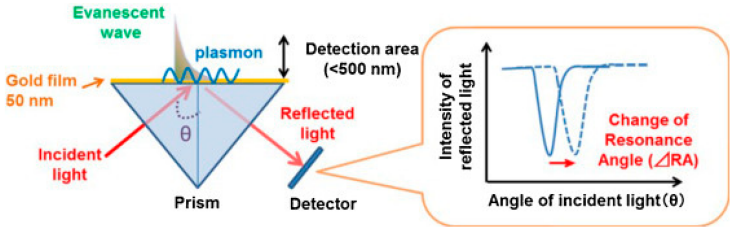

Figure 2. Schematic description of SPR sensor.

2.1. SPR-Coupled ECL

To provide a deep understanding of the interaction between SPR and ECL, Dinel et al. reported the first combination of SPR and ECL techniques to investigate the interfacial adsorption and energy transfer processes between ECL and the plasmonic substrate [53]. In this work, the ECL evolution on a classic Au chip for SPR measurements was employed under the irradiation of external LED light for the excitation of SPR. Tween 80 was used as a protective layer on the gold film. The real-time monitoring capabilities enabled studies on the impact of plasmon resonance on the ECL process of $Ru(bpy)_3^{2+}$. Various control experiments demonstrated that SPR and ECL can be detected simultaneously without interference. ECL intensity was quenched in the presence of illumination of the SPR chip because the activated plasmon reduced the probability of radiative relaxation of the excited luminophore. This phenomenon indicated that ECL emission occurred very close to the electrode surface after being modified by Tween 80. The combination of SPR and ECL provided fundamental insights into the mechanism of interfacial processes involving electrochemical reactions and electrode passivation.

The requirement of sophisticated apparatus and complex optics of the conventional Kretschmann prism-based SPR setup inhibits applications in sensing and online monitoring. To provide an easier configuration, Yu et al. designed a flow injection ESPR device (**Figure 3**) through a new electrochemical SPR conductive fiber where a gold nanohole array film was integrated [54]. This configuration enabled direct collection of the plasmonic response in transmission mode. Considering the portability and low cost of the fiber-based probe, the co-reactant-based ECL system, including $Ru(bpy)_3^{2+}$ and TPrA, was tested to provide interfacial SPR information and mechanistic insights into the ECL process. The SPR signal directly revealed the oxidation reaction of TPrA in the vicinity of the electrode surface due to the change in the local refractive index.

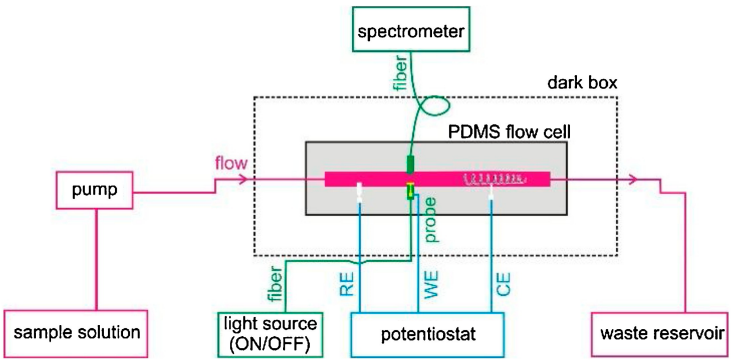

Figure 3. Assembly schematic diagram of the flow injection fiber optic ESPR device.

2.2. LSPR-coupled ECL

In addition to SPR generated on two-dimension gold film, LSPR generated on zero-dimension or one-dimension gold nanomaterials was more commonly used to regulate ECL emission. The enhanced ECL efficiency by LSPR was determined in the presence of citrate-coated gold nanoparticle aqueous solutions [55]. The classic ECL reactions between $Ru(bpy)_3^{2+}$ and oxalate were tested in an aqueous solution containing 5 nm gold nanoparticles. The SPR band of gold nanoparticles solution showed a red-shift in the presence of $Ru(bpy)_3^{2+}$, which indicated the nanoparticle aggregation and promoted the SPR-ECL coupling effect with 620 nm ECL emission of $Ru(bpy)_3^{2+}$. The integrated ECL emission was increased by approximately 3-fold compared with its value in the absence of gold nanoparticles. Although gold nanomaterials are known to be able to improve the electrochemical rate, the direct observation of ECL enhancement at single gold nanomaterials was not realized yet. Therefore, Pan et al. discovered that ECL intensity was enhanced with the increase in the size of gold nanoparticles with ECL microscopy [56]. Thanks to the spatial and temporal resolution of ECL microscopy, the local ECL signal from different gold nanoparticles with time elapsing were recorded in a high throughput manner. Two kinds of gold nanoparticles, namely, electrodeposited and pre-synthesized gold nanoparticles, both showed ECL enhancement, but electrodeposited gold nanoparticles showed a narrow ECL intensity distribution. In addition, ECL microscopy was used to study the plasmon-enhanced ECL at the level of a single nanoparticle based on the ordered array of Au NPs (**Figure 4**a) [57]. Thanks to the establishment of the precise location and a high throughput platform, LSPR led to the increased ECL by large Au NPs (>80 nm) in the $Ru(bpy)_3^{2+}$/TPrA system, which was related with the Au NP configuration and sizes. The coupled Au NPs demonstrated higher ECL strength compared with the uncoupled ones, which was consistent with numerical simulations. This plasmon-enhanced ECL imaging strategy can be used in single-particle electrocatalysis in the future.

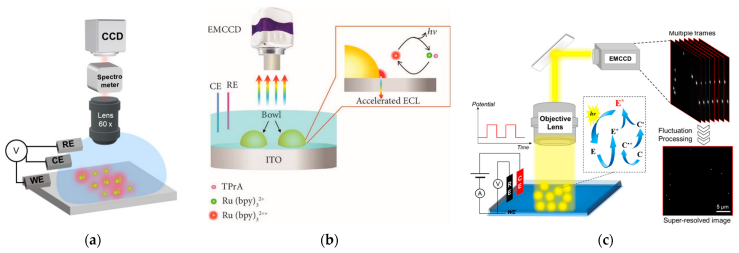

Figure 4. (**a**) Schematic illustration of ECL microscopy for imaging an Au NP array with a 5 μm interval. (**b**) Schematic representation of the electrochemiluminescence imaging. The luminophore, $Ru(bpy)_3^{2+}$, and co-reactant, TPrA, are oxidized at the heterogeneous interface between the microbowls and the ITO supporting electrode with the aid of an enhanced electric field, generating the excited state $Ru(bpy)_3^{2+*}$. The accelerated ECL emission is produced during the relaxation of $Ru(bpy)_3^{2+*}$ back to the ground state. (**c**) Schematic illustration of the ECLM system for single-particle imaging and basic principle of SRRF analysis of multiple images.

Spectral overlap between nanoparticle scattering and ECL emission was considered as a prerequisite to generate surface plasmon coupling ECL. Although many reports based on ensemble spectroscopy demonstrated that plasmonic nanostructures can act as signal boosting antennas to amplify ECL, single-nanoparticle heterogeneities and the structure–function relationship remain uncovered. To provide insight into the spectral overlap at the single-particle level, Heiderscheit et al. investigated the influence of nano-emitter spectral overlap under the microscopic view [58]. It was found that those nanoparticles with a larger spectral overlap between scattering and ECL showed stronger ECL enhancement. The measurement at the single particle level excluded the influence from adjacent particles and the average effect. The ECL intensity can be increased up to 10-fold at the maximal spectral overlap using either gold nanoparticles or gold nanotriangles. In addition to spectral overlap, Cui et al. found that an enhanced electric field also boosted the ECL signal. They fabricated a heterogeneous interface by loading bowl-like gold particles on the indium tin oxide (ITO) substrate electrode (**Figure 4**b) [47]. The heterointerface between the gold bowl and ITO produced an enhanced electric field, which caused a bright ECL ring around the gold bowl. COMSOL simulations showed similar results with the captured ECL patterns from EMCCD. This work suggested that the heterogeneous distribution of the electric field effect could serve as a new mechanism to accelerate the electrocatalytic reaction rate as well as the relevant ECL intensity in biosensors.

Although isolated noble metal particles have been often used to test the surface plasmonic ECL effect, periodic particle arrays with surface lattice resonances can also regulate the luminescence properties in many cases. Heiderscheit et al. further demonstrated that the hexagonally packed arrays of gold nanodisks enhanced the ECL of $Ru(bpy)_3^{2+}$ and TPrA [59]. Both theoretical and experimental results confirmed that the nanodisk spacing and measurement geometry affected the ECL enhancement factors. After measuring the ECL intensity and spectrum under all lattice spacings, a 24-fold ECL

intensity enhancement was found with no deviation in the $Ru(bpy)_3^{2+}$ spectrum. A theoretical prediction showed that ECL could be further enhanced when $Ru(bpy)_3^{2+}$ was closer to the gold array.

Under the condition of ECL measurements, the surface oxide of gold nanomaterials can be formed at a high anodic potential. This surface oxide layer can hinder the electron transfer rate and gradually decrease the ECL intensity, leading to poor stability at repeat measurements. Wilson et al. investigated the ECL scenario generated with single gold nanowire [60]. The as-purchased nanowires did not show any ECL signal due to the block of surface hexadecyltrimethylammonium surfactant. After removing the surfactant and coating the nanowires with a protective polymer blend, gold nanowires showed a better ECL stability because the polymer layer protected the gold surface from electrochemical oxidation and damage. In addition, the polymer thickness significantly influenced the sharpness and reproducibility of ECL images during ECL measurement.

Because the distribution of electrocatalytic activity at single nanomaterials is heterogeneous, it is important to map the ECL signal at the sub-particle level. The uneven electrocatalytic activity on individual 2D gold nanoplates was imaged with submicron resolution [49]. Because of different electrocatalytic rates at different sites, the corners, edges, and flat facet showed a non-uniform ECL distribution. Although much higher ECL intensity was observed at the corners and edges with more defect sites, the flat facet possessed higher ECL stability with time elapsing. To break the optical diffraction limit in ECL microscopy, Chen et al. subsequently develop super-resolution ECL microscopy with a radial fluctuation algorithm (**Figure 4**c) [48]. The stochastic nature of the ECL emission made the generated photons obey Poisson statistics. The Poisson distribution benefited the super-resolution radial fluctuation algorithm, providing more abundant details on gold nanomaterials with 100 nm spatial resolution. The super-resolution imaging technique provided more detailed electrocatalytic sites on single gold nanospheres, nanorods, and nanoplates. In addition to optical fluctuation imaging methods, single-molecular localization microscopy can also be used to obtain super-resolution image of gold plates. Dong et al. used single-molecule ECL microscopy for mapping chemical activity and reaction kinetics on single gold plates [61]. The high spatial resolution (37 nm) and temporal resolution enabled the trace of dynamic evolution of catalytic sites as a function of time.

References

1. Ma, C.; Cao, Y.; Gou, X.; Zhu, J.J. Recent Progress in Electrochemiluminescence Sensing and Imaging. Anal. Chem. 2020, 92, 431–454.
2. Jiang, J.; Lin, X.; Ding, D.; Diao, G. Graphitic-phase carbon nitride-based electrochemiluminescence sensing analyses: Recent advances and perspectives. RSC Adv. 2018, 8, 19369–19380.
3. Valenti, G.; Rampazzo, E.; Kesarkar, S.; Genovese, D.; Fiorani, A.; Zanut, A.; Palomba, F.; Marcaccio, M.; Paolucci, F.; Prodi, L. Electrogenerated chemiluminescence from metal complexes-based nanoparticles for highly sensitive sensors applications. Coord. Chem. Rev. 2018, 367, 65–81.
4. Zhang, S.; Liu, Y. Recent Progress of Novel Electrochemiluminescence Nanoprobes and Their Analytical Applications. Front. Chem. 2020, 8, 626243.
5. Zanut, A.; Fiorani, A.; Rebeccani, S.; Kesarkar, S.; Valenti, G. Electrochemiluminescence as emerging microscopy techniques. Anal. Bioanal. Chem. 2019, 411, 4375–4382.
6. Ding, H.; Su, B.; Jiang, D. Recent Advances in Single Cell Analysis by Electrochemiluminescence. ChemistryOpen 2022, 2022, e202200113.
7. Knezevic, S.; Bouffier, L.; Liu, B.; Jiang, D.; Sojic, N. Electrochemiluminescence microscopy: From single objects to living cells. Curr. Opin. Electrochem. 2022, 35, 101096.
8. Rebeccani, S.; Zanut, A.; Santo, C.I.; Valenti, G.; Paolucci, F. A Guide Inside Electrochemiluminescent Microscopy Mechanisms for Analytical Performance Improvement. Anal. Chem. 2022, 94, 336–348.
9. Zhou, J.H.; Zhang, S.Y.; Liu, Y. Electrochemiluminescence Single-cell Analysis on Nanostructured Interface. Electroanal 2022, 34, 937–946.
10. Zhang, Z.; Ma, C.; Xu, Q.; Zhu, J.-J. Recent progress in electrochemiluminescence microscopy analysis of single cells. Analyst 2022, 147, 2884–2894.
11. Fereja, T.H.; Du, F.; Wang, C.; Snizhko, D.; Guan, Y.; Xu, G. Electrochemiluminescence Imaging Techniques for Analysis and Visualizing. J. Anal. Test. 2020, 4, 76–91.
12. Lv, X.; Li, Y.; Cui, B.; Fang, Y.; Wang, L. Electrochemiluminescent sensor based on an aggregation-induced emission probe for bioanalytical detection. Analyst 2022, 147, 2338–2354.

13. Wei, X.; Zhu, M.J.; Yan, H.; Lu, C.; Xu, J.J. Recent Advances in Aggregation-Induced Electrochemiluminescence. Chem. A Eur. J. 2019, 25, 12671–12683.

14. Chen, Y.; Cao, Y.; Ma, C.; Zhu, J.-J. Carbon-based dots for electrochemiluminescence sensing. Mater. Chem. Front. 2020, 4, 369–385.

15. Ma, C.; Wu, W.; Peng, Y.; Wang, M.X.; Chen, G.; Chen, Z.; Zhu, J.J. A Spectral Shift-Based Electrochemiluminescence Sensor for Hydrogen Sulphide. Anal. Chem. 2018, 90, 1334–1339.

16. Zou, R.; Teng, X.; Lin, Y.; Lu, C. Graphitic carbon nitride-based nanocomposites electrochemiluminescence systems and their applications in biosensors. TrAC Trends Anal. Chem. 2020, 132, 116054.

17. Xue, J.; Zhang, Z.; Zheng, F.; Xu, Q.; Xu, J.; Zou, G.; Li, L.; Zhu, J.-J. Efficient Solid-State Electrochemiluminescence from High-Quality Perovskite Quantum Dot Films. Anal. Chem. 2017, 89, 8212–8216.

18. Cao, Y.; Zhu, W.; Wei, H.; Ma, C.; Lin, Y.; Zhu, J.-J. Stable and Monochromatic All-Inorganic Halide Perovskite Assisted by Hollow Carbon Nitride Nanosphere for Ratiometric Electrochemiluminescence Bioanalysis. Anal. Chem. 2020, 92, 4123–4130.

19. Han, T.; Cao, Y.; Wang, J.; Jiao, J.; Song, Y.; Wang, L.; Ma, C.; Chen, H.-Y.; Zhu, J.-J. Crystallization-Induced Enhanced Electrochemiluminescence from a New Tris(bipyridine)ruthenium(II) Derivative. Adv. Funct. Mater. 2023, 2023, 2212394.

20. Cai, W.-R.; Zeng, H.-B.; Xue, H.-G.; Marks, R.S.; Cosnier, S.; Zhang, X.-J.; Shan, D. Enhanced Electrochemiluminescence of Porphyrin-Based Metal–Organic Frameworks Controlled via Coordination Modulation. Anal. Chem. 2020, 92, 1916–1924.

21. Bezuneh, T.T.; Fereja, T.H.; Kitte, S.A.; Li, H.; Jin, Y. Gold nanoparticle-based signal amplified electrochemiluminescence for biosensing applications. Talanta 2022, 248, 123611.

22. Chu, Y.; Han, T.; Deng, A.; Li, L.; Zhu, J.-J. Resonance energy transfer in electrochemiluminescent and photoelectrochemical bioanalysis. Trac-Trends Anal. Chem. 2020, 123, 115745.

23. Li, L.; Chen, Y.; Zhu, J.J. Recent Advances in Electrochemiluminescence Analysis. Anal. Chem. 2017, 89, 358–371.

24. Cao, Y.; Ma, C.; Zhu, J.-J. DNA Technology-assisted Signal Amplification Strategies in Electrochemiluminescence Bioanalysis. J. Anal. Test. 2021, 5, 95–111.

25. Ma, C.; Wu, S.; Zhou, Y.; Wei, H.-F.; Zhang, J.; Chen, Z.; Zhu, J.-J.; Lin, Y.; Zhu, W. Bio-Coreactant-Enhanced Electrochemiluminescence Microscopy of Intracellular Structure and Transport. Angew. Chem. 2021, 60, 4907–4914.

26. Guo, W.; Zhou, P.; Sun, L.; Ding, H.; Su, B. Microtube Electrodes for Imaging the Electrochemiluminescence Layer and Deciphering the Reaction Mechanism. Angew. Chem. 2021, 60, 2089–2093.

27. Wang, Q.; Ren, Z.H.; Zhao, W.M.; Wang, L.; Yan, X.; Zhu, A.S.; Qiu, F.M.; Zhang, K.K. Research advances on surface plasmon resonance biosensors. Nanoscale 2022, 14, 564–591.

28. Pan, S.; Li, X.; Yadav, J. Single-nanoparticle spectroelectrochemistry studies enabled by localized surface plasmon resonance. Phys. Chem. Chem. Phys. 2021, 23, 19120–19129.

29. Mouloua, D.; Kotbi, A.; Deokar, G.; Kaja, K.; El Marssi, M.; El Khakani, M.A.; Jouiad, M. Recent Progress in the Synthesis of MoS(2) Thin Films for Sensing, Photovoltaic and Plasmonic Applications: A Review. Materials 2021, 14, 3283.

30. Gong, L.; Feng, L.; Zheng, Y.; Luo, Y.; Zhu, D.; Chao, J.; Su, S.; Wang, L. Molybdenum Disulfide-Based Nanoprobes: Preparation and Sensing Application. Biosensors 2022, 12, 87.

31. Dao, T.D.; Han, G.; Arai, N.; Nabatame, T.; Wada, Y.; Hoang, C.V.; Aono, M.; Nagao, T. Plasmon-mediated photocatalytic activity of wet-chemically prepared ZnO nanowire arrays. Phys. Chem. Chem. Phys. 2015, 17, 7395–7403.

32. Guo, L.; Yin, H.; Xu, M.; Zheng, Z.; Fang, X.; Chong, R.; Zhou, Y.; Xu, L.; Xu, Q.; Li, J.; et al. In Situ Generated Plasmonic Silver Nanoparticle-Sensitized Amorphous Titanium Dioxide for Ultrasensitive Photoelectrochemical Sensing of Formaldehyde. ACS Sens. 2019, 4, 2724–2729.

33. Zheng, Z.; Murakami, N.; Liu, J.; Teng, Z.; Zhang, Q.; Cao, Y.; Cheng, H.; Ohno, T. Development of Plasmonic Photocatalyst by Site-selective Loading of Bimetallic Nanoparticles of Au and Ag on Titanium(IV) Oxide. ChemCatChem 2020, 12, 3783–3792.

34. Li, M.; Singh, R.; Soares, M.S.; Marques, C.; Zhang, B.; Kumar, S. Convex fiber-tapered seven core fiber-convex fiber (CTC) structure-based biosensor for creatinine detection in aquaculture. Opt. Express 2022, 30, 13898–13914.

35. Wang, Y.; Singh, R.; Chaudhary, S.; Zhang, B.; Kumar, S. 2-D Nanomaterials Assisted LSPR MPM Optical Fiber Sensor Probe for Cardiac Troponin I Detection. IEEE Trans. Instrum. Meas. 2022, 71, 1–9.

36. Wang, Z.; Singh, R.; Marques, C.; Jha, R.; Zhang, B.; Kumar, S. Taper-in-taper fiber structure-based LSPR sensor for a lanine aminotransferase detection. Opt. Express 2021, 29, 43793–43810.

37. Wang, Z.; Singh, R.; Zhang, B.; Kumar, S. SMF tapered fiber/AuNPs/ZnO based sensor for detection of acetylcholine. I n Optics in Health Care and Biomedical Optics XI; Luo, Q., Li, X., Gu, Y., Zhu, D., Eds.; Spie-Int Soc Optical Engineerin g: Bellingham, WA, USA, 2021; Volune 11900, p. 119003D.

38. Kumar, S.; Singh, R.; Kaushik, B.K.; Chen, N.-k.; Yang, Q.S.; Zhang, X. LSPR-Based Cholesterol Biosensor Using Holl ow Core Fiber Structure. IEEE Sens. J. 2019, 19, 7399–7406.

39. Singh, L.; Singh, R.; Zhang, B.; Cheng, S.; Kumar Kaushik, B.; Kumar, S. LSPR based uric acid sensor using graphene oxide and gold nanoparticles functionalized tapered fiber. Opt. Fiber Technol. 2019, 53, 102043.

40. Kumar, S.; Wang, Y.; Li, M.Y.; Wang, Q.L.; Malathi, S.; Marques, C.; Singh, R.; Zhang, B.Y. Plasmon-Based Tapered-in-Tapered Fiber Structure for p-Cresol Detection: From Human Healthcare to Aquaculture Application. Ieee Sens. J. 202 2, 22, 18493–18500.

41. Su, Y.; Xu, S.; Zhang, J.; Chen, X.; Jiang, L.-P.; Zheng, T.; Zhu, J.-J. Plasmon Near-Field Coupling of Bimetallic Nanost ars and a Hierarchical Bimetallic SERS “Hot Field”: Toward Ultrasensitive Simultaneous Detection of Multiple Cardioren al Syndrome Biomarkers. Anal. Chem. 2019, 91, 864–872.

42. Wen, S.; Su, Y.; Dai, C.; Jia, J.; Fan, G.-C.; Jiang, L.-P.; Song, R.-B.; Zhu, J.-J. Plasmon Coupling-Enhanced Raman S ensing Platform Integrated with Exonuclease-Assisted Target Recycling Amplification for Ultrasensitive and Selective D etection of microRNA-21. Anal. Chem. 2019, 91, 12298–12306.

43. Wang, Z.; Xue, J.; Bi, C.; Xin, H.; Wang, Y.; Cao, X. Quantitative and specific detection of cancer-related microRNAs in living cells using surface-enhanced Raman scattering imaging based on hairpin DNA-functionalized gold nanocages. A nalyst 2019, 144, 7250–7262.

44. Lu, D.; Xia, J.; Deng, Z.; Cao, X. Detection of squamous cell carcinoma antigen in cervical cancer by surface-enhanced Raman scattering-based immunoassay. Anal. Methods 2019, 11, 2809–2818.

45. Su, Y.-w.; Wang, W. Surface plasmon resonance sensing: From purified biomolecules to intact cells. Anal. Bioanal. Che m. 2018, 410, 3943–3951.

46. Li, J.; Qi, H.; Wang, H.; Yang, Z.; Zhu, P.; Diao, G. Fluorescence energy transfer-based multiplexed hybridization assay using gold nanoparticles and quantum dot conjugates on photonic crystal beads. Microchim. Acta 2014, 181, 1109–111 5.

47. Cui, C.; Jin, R.; Jiang, D.; Zhang, J.; Zhu, J. Visualization of an Accelerated Electrochemical Reaction under an Enhanc ed Electric Field. Research 2021, 2021, 1742919.

48. Chen, M.M.; Xu, C.H.; Zhao, W.; Chen, H.Y.; Xu, J.J. Super-Resolution Electrogenerated Chemiluminescence Microsco py for Single-Nanocatalyst Imaging. J. Am. Chem. Soc. 2021, 143, 18511–18518.

49. Chen, M.M.; Zhao, W.; Zhu, M.J.; Li, X.L.; Xu, C.H.; Chen, H.Y.; Xu, J.J. Spatiotemporal imaging of electrocatalytic acti vity on single 2D gold nanoplates via electrogenerated chemiluminescence microscopy. Chem. Sci. 2019, 10, 4141–41 47.

50. Wang, P.; Zhao, J.; Wang, Z.; Liang, Z.; Nie, Y.; Xu, S.; Ma, Q. Polarization-Resolved Electrochemiluminescence Senso r Based on the Surface Plasmon Coupling Effect of a Au Nanotriangle-Patterned Structure. Anal. Chem. 2021, 93, 1578 5–15793.

51. Xia, J.; Zhou, J.; Zhang, R.; Jiang, D.; Jiang, D. Gold-coated polydimethylsiloxane microwells for high-throughput electr ochemiluminescence analysis of intracellular glucose at single cells. Anal. Bioanal. Chem. 2018, 410, 4787–4792.

52. Villani, E.; Valenti, G.; Marcaccio, M.; Mattarozzi, L.; Barison, S.; Garoli, D.; Cattarin, S.; Paolucci, F. Coreactant electro chemiluminescence at nanoporous gold electrodes. Electrochim. Acta 2018, 277, 168–175.

53. Dinel, M.P.; Tartaggia, S.; Wallace, G.Q.; Boudreau, D.; Masson, J.F.; Polo, F. The Fundamentals of Real-Time Surface Plasmon Resonance/Electrogenerated Chemiluminescence. Angew. Chem. Int. Ed. 2019, 58, 18202–18206.

54. Yu, J.; Jia, P.; Wang, S.; Ebendorff-Heidepriem, H.; Abell, A.D. Electrochemical plasmonic optical fiber probe for real-ti me insight into coreactant electrochemiluminescence. Sens. Actuators B Chem. 2020, 321, 128469.

55. Perez-Tejeda, P.; Grueso, E.; Marin-Gordillo, A.; Torres-Marquez, C.; Giraldez-Perez, R.M. Aqueous Gold Nanoparticle Solutions for Improved Efficiency in Electrogenerated Chemiluminescent Reactions. Acs. Appl. Nano. Mater. 2018, 1, 5 307–5315.

56. Pan, S.; Liu, J.; Hill, C.M. Observation of Local Redox Events at Individual Au Nanoparticles Using Electrogenerated C hemiluminescence Microscopy. J. Phys. Chem. C 2015, 119, 27095–27103.

57. Wei, Y.; Zhang, Y.; Pan, J.; Chen, T.; Xing, X.; Zhang, W.; Lu, Z. Plasmon-Enhanced Electrochemiluminescence at the Single-Nanoparticle Level. Angew. Chem. 2022, 2022, e202214103.
58. Heiderscheit, T.S.; Gallagher, M.J.; Baiyasi, R.; Collins, S.S.E.; Jebeli, S.A.H.; Scarabelli, L.; Al-Zubeidi, A.; Flatebo, C.; Chang, W.-S.; Landes, C.F.; et al. Nanoelectrode-emitter spectral overlap amplifies surface enhanced electrogenerated chemiluminescence. J. Chem. Phys. 2019, 151, 144712.
59. Heiderscheit, T.S.; Oikawa, S.; Sanders, S.; Minamimoto, H.; Searles, E.K.; Landes, C.F.; Murakoshi, K.; Manjavacas, A.; Link, S. Tuning Electrogenerated Chemiluminescence Intensity Enhancement Using Hexagonal Lattice Arrays of Go ld Nanodisks. J. Phys. Chem. Lett. 2021, 12, 2516–2522.
60. Wilson, A.J.; Marchuk, K.; Willets, K.A. Imaging Electrogenerated Chemiluminescence at Single Gold Nanowire Electro des. Nano Lett. 2015, 15, 6110–6115.
61. Dong, J.; Xu, Y.; Zhang, Z.; Feng, J. Operando Imaging of Chemical Activity on Gold Plates with Single-Molecule Electr ochemiluminescence Microscopy. Angew. Chem. 2022, 2022, e202200187.